RSC Advances

ROYAL SOCIETY OF CHEMISTRY

www.rsc.org/advances

Journal Name

ARTICLE

Vertically Aligned Carbon Nanotubes@MnO_2 Nanosheets Arrays Grown on Carbon Cloth for High Performance Flexible Electrodes of Supercapacitors

Received 00th January 20xx,
Accepted 00th January 20xx

DOI: 10.1039/x0xx00000x

www.rsc.org/

Xiao-Jun Li[a,b], Yong Zhao[b], Wei-Guo Chu[b], Yue Wang[b], Zhen-Jun Li[b], Peng Jiang*[b], Xiu-Chen Zhao*[a], Minghui Liang*[b], Ying Liu[a]

The vertical alligned carbon nanotubes@MnO_2 (VACNTs@MnO_2) arrays grown on carbon cloth was prepared as high performance flexible electrodes for supercapacitors. VACNTs first grew on carbon cloth with the method of plasma enhanced chemical vapor deposition (PECVD) to obtain firm connection between CNTs and carbon cloth, and δ-MnO_2 nanosheets were deposited on the surface of VACNTs to form VACNTs@MnO_2 core-shell structure. The VACNTs@MnO_2 on carbon cloth (VACNTs@MnO_2/CC) exhibited a remarkable specific capacitance (235 F g^{-1} at the scan rate of 2 mV s^{-1} based on the total mass of VACNTs and MnO_2), an excellent rate performance with a specific capacitance of 188 F g^{-1} at 100 mV s^{-1} and a stable cycling ability (nearly 100% retention after 5000 charge/discharge cycles at 5 A g^{-1}). The fabricated symmetric supercapacitor from the self-support VACNTs@MnO_2/CC without any additive reagents had same electrochemical energy storage performance when this supercapacitor was bent for 180°, revealing the excellent flexibility of our prepared flexible electrodes.The excellent performances in electrochemical properties and flexibility mainly originated from a strong mechanical coupling between CNTs and CC as well as the sufficient contact between electrolyte and the surface of MnO_2 nanosheets in such an arrayed structure.

Introduction

To develop high performance flexible supercapacitors is of great importance for meeting the energy demands for future wearable electronic devices.[1-6] The parameters of supercapacitors including specific capacitance, energy density, power density, rate capacitance, and cycling life are key factors influencing the practical applications of supercapacitors, especially for flexible supercapacitors. Pseudocapacitors as a kind of supercapacitor typically have higher specific capacitance than that of electrical double-layer capacitors (EDLCs) because the electrode materials for pseudocapacitors, such as metal oxides of RuO_2, MnO_2 and NiO, store electric energy with redox reactions and have high theoretical capacitances.[7-10] However, except for RuO_2, most of metal oxides for the electrode of pseudocapacitors have poor conductivities, which leads to the limited specific capacitances are observed during charge-discharge process because the redox reactions of these metal oxides only occur on their shallow surfaces.[11-14] To solve this problem, some conductive materials, such as conductive polymers, graphene, and CNTs have been used to corporate with these metal oxides, and the performance of the metal oxide-based supercapacitors can be enhanced through this route.[15-21]

MnO_2 is a kind of promising electrode material for supercapacitors with large theoretical specific capacitance (1370 F·g^{-1}), natural abundance, low cost and environmental friendliness, thus to develop MnO_2-based flexible supercapacitors is highly desirable. The contributions to increase the conductivity of MnO_2 materials have been made. For example, Feng et al used CNTs and poly(3,4-ethylenedioxythiophene (PEDOT) to enhance the conductivity of MnO_2 and the enhanced electrode performance was obtained.[22] Li's group reported the high specific capacitance of flexible MnO_2-based electrode with the addition of the highly conductive Zn_2SnO_4.[23] Besides the addition of conductive materials in the MnO_2-based electrode to improve its specific capacitance, the morphology of MnO_2 is also an important factor.[24-27] MnO_2 nanosheet is a good choice to enhance its specific capacitance because this kind of morphology facilitates the redox reaction of MnO_2.[28,29] Furthermore, the flexible substrates, such as carbon cloth and carbon fiber papers, are promising for fabrication of flexible electrodes in supercapacitors because of their excellent conductivity and flexibility.[30-32] However, the efficient combination between

[a] School of Materials Science & Engineering, Beijing Institute of Technology, Beijing 100081, China. E-mail: zhaoxiuchen@bit.edu.cn
[b] National Center for Nanoscience and Technology (NCNST), Beijing 100190, P. R. China. E-mail: pjiang@nanoctr.cn; liangmh@nanoctr.cn; Fax: +86 (10) 62656765
Electronic Supplementary Information (ESI) available: [TEM images, Raman spectra, XRD, electrochemical characterizations of CNTs/CC and the driven LED light]. See DOI: 10.1039/x0xx00000x

flexible substrates and MnO_2-based electrode is necessary to resist bending activity during the practical applications, in order to avoid the resulted capacitance decaying and lifetime shortening of flexible supercapacitors.

Based on above consideration, a new route to prepare the flexible MnO_2-based electrode for supercapacitors was set up, which included the growth of vertically aligned carbon nanotubes (VACNTs) arrays on carbon cloth and the subsequent deposition of δ-MnO_2 nanosheets on CNTs (Scheme 1). The grown VACNTs arrays played double roles of support and conductive materials for MnO_2, which also made the flexible electrode robust. This flexible electrode exhibited high specific capacitance, high rate capacitance and excellent cycling performance according to our measurement results.

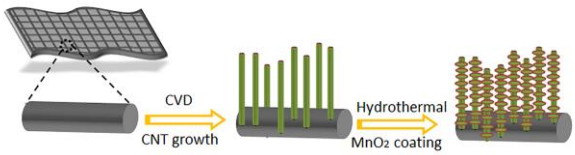

Scheme 1. The preparation route of vertically aligned carbon nanotubes@MnO_2 arrays over carbon cloth.

Results and discussion

Carbon cloth (CC) was used the flexible current collector for supercapacitors in our work. The carbon nanotubes (CNTs) were grown on CC to bridge MnO_2 and CC for two reasons; one is to obtain firm connection between current collectors and active materials, and another is that CNTs play the role of conductive channels. The uniform arrangement of CNTs arrays had vacancy to allow the deposition of active materials for supercapacitors. Figure 1 shows the SEM images of the as-prepared VACNTs-arrays and VACNTs@MnO_2 grown on carbon cloth (CC). The vertically aligned CNTs arrays on the CC can be clearly seen in Fig. 1a and 1b. The diameters and lengths of most of the CNTs are in the range of 105~130 nm and 2~5μm, respectively. Figure 1c and 1d demonstrate the morphologies of the composite VACNTs@MnO_2 on CC obtained by treating VACNTs on CC with 10 mM $KMnO_4$ aqueous solution at 180℃ for 30 minutes. It can be clearly observed that the ultrathin MnO_2 nanosheets formed a layer of porous three-dimensional networks on the surfaces of the CNTs. The production of the MnO_2 nanosheets on the CNTs probably mainly resulted from the chemical reaction between $KMnO_4$ and the amorphous carbon formed on the CNT surfaces.[33] Because we observed amorphous carbon of about 1 nm thickness on the surface of CNT in the high-resolution TEM image (Figure S1a). The strong D peak in Raman spectra of the CNTs (Figure S1b) also indicated the existence of amorphous carbon.

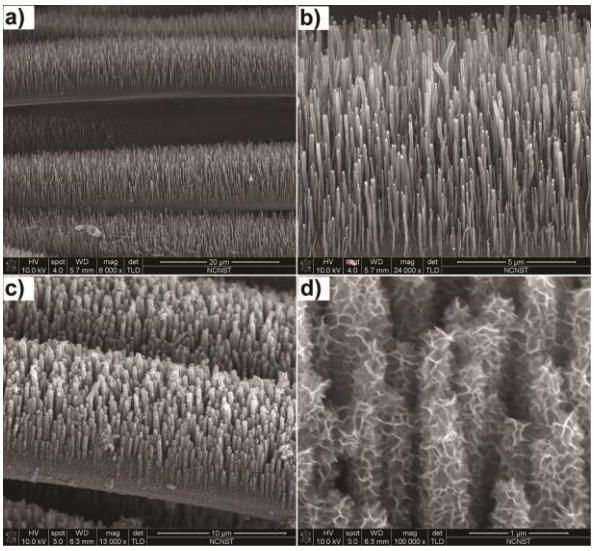

Fig.1 a) The SEM image of vertically aligned carbon nanotubes (VACNTs) grown on carbon cloth; b) the enlarged image of a); c) The SEM image of VACNTs@MnO_2 on CC; d) The enlarged image of c).

The prepared VACNTs@MnO_2 composite was further characterized by TEM (Fig. 2). The structure of porous MnO_2 wrapped CNT can be seen in Figure 2a. The average thickness of the MnO_2 nanosheets composed shell was about 60 nm. The element mapping (Figure 3c-e) in the region of Figure 3b demonstrates the distribution of various elements C, O, and Mn in the composite, indicating the formation of the VACNTs@MnO_2 core-shell nanostructure. These elements can also be observed in the EDS spectrum of Figure S2. Figure S3 shows a high-resolution TEM image of the MnO_2 nanosheets, and the nanosized MnO_2 crystals can be observed. The inset in Figure S3 provides selected area electronic diffraction (SAED) pattern of the strip area. The atomic layer inter-distance was measured to be about 0.7 nm, belonging to that of (001) planes for δ–MnO_2. The X-ray diffraction pattern of the VACNTs@MnO_2 composites also confirmed the presence of crystalline δ–MnO_2 (Fig. S4). A broad weak peak around 37° in XRD can be indexed to δ–MnO_2 (111) planes (JCPDS 42-1317).

To know the chemical component and surface chemical states of the VACNTs@MnO_2 composite on CC, X-ray photoelectron spectroscopy (XPS) measurement was carried out. Figure 3a and 3b display the Mn_{2p} and O_{1s} spectra for the composite, respectively. The Mn_{2p} spectrum presents two main peaks locating at 642.1 and 653.7 eV, being assigned to $Mn_{2p3/2}$ and $Mn_{2p1/2}$ for Mn^{4+} in MnO_2, respectively. Meanwhile, the signals of Mn^{3+} and Mn^{5+} species can also be observed in the spectrum. In the O_{1s} region, there have three peaks with the binding energies of 529.9, 530.8 and 531.8 eV. The sharp peak located at 529.9 eV is for O element in Mn-O-Mn oxide, other two side peaks at 530.8 and 531.8 eV correspond to O element in hydroxide (Mn-O-H) and water (H-O-H).

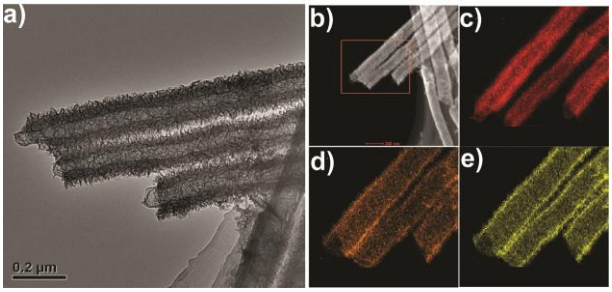

Fig. 2a) The TEM image of VACNTs@MnO_2 ; b) The STEM image of VACNTs@MnO_2; The element mapping of c) C, d) O, and e) Mn in the selected area in b).

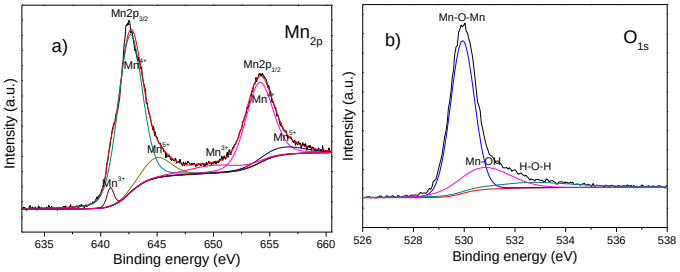

Fig.3 The XPS spectra of a) Mn_{2p} and b) O_{1s} for the VACNTs@MnO_2 composite

Electrochemical performance of the VACNTs@MnO_2 composite on CC (VACNTs@MnO_2/CC) electrodes was explored in three-electrode system and two-electrode system, respectively. The VACNTs@MnO_2/CC electrode can be directly used as a work electrode without any additive reagents, a saturated calomel electrode (SCE) as a reference and a platinum foil as a counter-electrode in the three-electrode system, respectively. For comparison, a VACNTs/CC electrode was also employed as a reference work electrode to detect electrochemical properties under the same conditions. Typically, the loading mass of CNT on carbon cloth for the measurements was 0.06 mg cm^{-2}, and that of MnO_2 was 0.20 mg cm^{-2} in our tested electrodes.

Figure 4a shows the cyclic voltammetry (CV) curves for the VACNTs@MnO_2/CC and CNTs/CC electrodes in 1.0 M Na_2SO_4 electrolyte between 0 and 0.8V (Vs. SCE) at a scan rate of 5 mVs^{-1}; The CNTs/CC electrode presented a much far lower specific capacitance (3.1 F g^{-1} at the scan rate of 5 mV s^{-1}, Figure S5) than that of the VACNTs@MnO_2/CC electrode (234 F g^{-1} at the scan rate of 5 mV s^{-1}, based on the total mass of CNTs and MnO_2). Figure 4b shows the typical CV curves of the VACNTs@MnO_2/CC electrode at different scan rates ranging from 2 to 100 mV s^{-1}. Quasi-rectangular shapes for all CV curves at different scan rates indicated ideal pseudo- and reversible capacitor behavior in the voltage window of 0~0.8 V versus SCE. It's worth mentioning that the specific capacitance at 2 mV s^{-1} (235 F g^{-1}) was nearly same as that at 5 mV s^{-1}. When the scan rate was 100 mVs^{-1}, the SC of the electrode reached 188 F g^{-1}. Figure 4c demonstrates the influence of current density on the measured specific capacitance (SC) of the VACNTs@MnO_2/CC electrode. A high SC of 263 F g^{-1} at 0.5 A g^{-1} can be obtained. It can reach 198 F g^{-1} even at a high current density of 20 A g^{-1}, exhibits a better SC than reported data concerning the MnO_2-CNTs electrodes.[20,21,34] Though the SC of VACNTs@MnO_2/CC is lower than some reported data[21,22], the VACNTs@MnO_2/CC electrode showed a more preferable rate capability than the previously reported results.[35-37] The inset in Figure 4c are the galvanostatic charge-discharge (GCD) curves at different current density from 0.5 to 20 A g^{-1}, in which all the curves show a good linear symmetry, implying a good electrochemical reversibility and capacitive performance. Figure 4d presents the cycling performance of the VACNTs@MnO_2/CC electrode at a large current density of 5 A g^{-1}. The capacitance retention is nearly 100 % at room temperature even after 5000 cycles, strongly evidencing the excellent long-term cycle stability and reliability of the VACNTs@MnO_2/CC electrode.

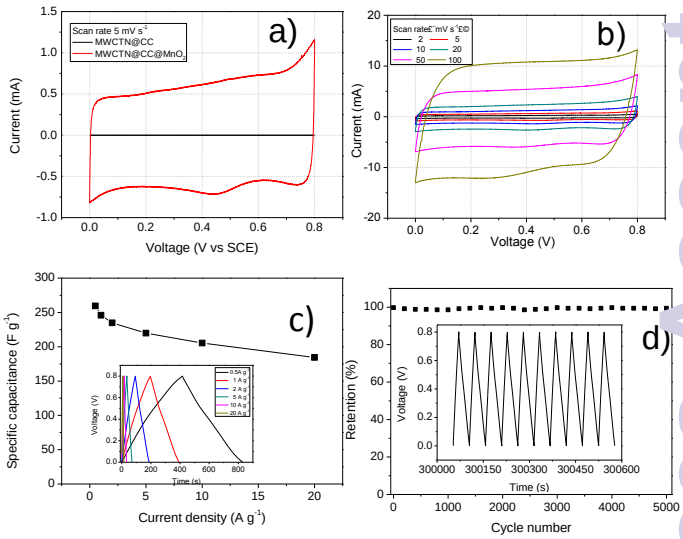

Fig. 4a) CV curves of the VACNTs/CC and VACNTs@MnO_2/CC at the scan rate of 5 mV s^{-1}; b) CV curves of VACNTs@MnO_2/CC at different scan rates ranging from 2 to 100mV s^{-1}; (c) Specific capacitance of VACNTs@MnO_2/CC as a function of current densities; d) The cycling performance of the VACNTs@MnO_2/CC electrode under the current density of 5 A g^{-1}, the inset presents the last ten cycles curves.

Furthermore, electrochemical impedance spectroscopy (EIS) was employed to detect the properties of charge and ion transport in the VACNTs@MnO_2/CC electrode. Figure 5 shows a Nyquist plot for the electrode. The EIS data in the Nyquist plot of Z'' versus Z' shows a nearly linear dependence. The slope of the line indicates the fast diffusive behaviours of the electrolyte in electrode pores and ions in active materials. The

equivalent series resistance (ESR) for the VACNTs@MnO_2/CC electrode was 3.3 Ω obtained from the Nyquist plot.[38, 39] The ESR can also be estimated as3.8 Ω by IR drops (Fig. S6) in Fig. 4c inset, which was very close to that from the Nyquist plot.

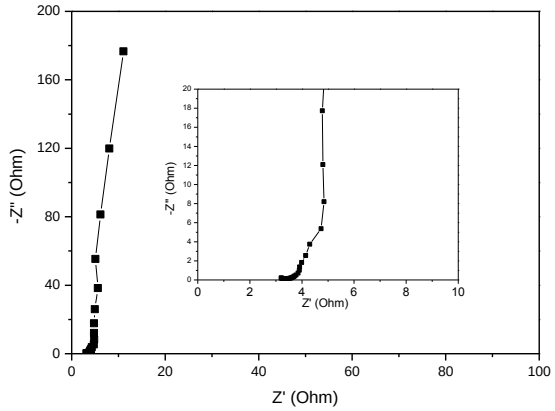

Fig. 5 Nyquist plot of VACNTs@MnO_2/CC tested from 100 kHz to 0.01 Hz with the amplitude of 5 mV. The inset is the enlarged figure of the Nyquist plot.

The symmetric supercapacitors based on the VACNTs@MnO_2/CC electrodes with aqueous Na_2SO_4 solution as electrolyte were assembled for the cyclic voltammetry and galvanostatic charge-discharge measurements. Figure 6a shows the typical CV curves at different scan rates from 2 to 100 mV s^{-1}. Similar to three–electrode system, all of CV curves show the quasi-rectangular shapes at different scan rates, suggesting ideal pseudo- and reversible capacitor behavior in the voltage window of 0~0.8 V. Figure 6b presents the SCs of the supercapacitor at various current density from 0.5 A g^{-1} to 20 A g^{-1}. The SC of 203.8 F/g at 0.5 A g^{-1} for symmetric supercapacitor can be obtained. Although the value of SCs at 0.5 A/g was lower than that in three-electrode system, the rate capacitance of this symmetric supercapacitor was better than that in three-electrode system. The specific capacitance can reach about 182 F g^{-1} at 20 A g^{-1}, holding the capacitance retention of 90% when the current density increased for 40 times.

To illustrate the flexibility of our VACNTs@MnO_2/CC electrode, a all-solid-state flexible supercapacitor (ASFS) (area was ~1.2 cm^2) based on this electrode was assembled; Two pieces of the VACNTs@MnO_2/CC electrodes were separated by a PVA-LiCl gel. Figure 7 shows the CV curves of this flexible device at the original state and the deformation angle of 180° at a scan rate of 50 mV s^{-1}. It can be seen that even if this flexible supercapacitor was bent for 180° the significant differences between its electrochemical behaviour and the original sample's behaviour cannot be found, revealing that the device possessed excellent electrochemical stability and deformation endurance. In addition, we tried the possibility of the VACNTs@MnO_2/CC-based flexible supercapacitor acting as power source for a LED light. Three ASFS in series can drive the LED red light after they were charged under the potential of 1.7 V for 8 seconds (Fig. S7).

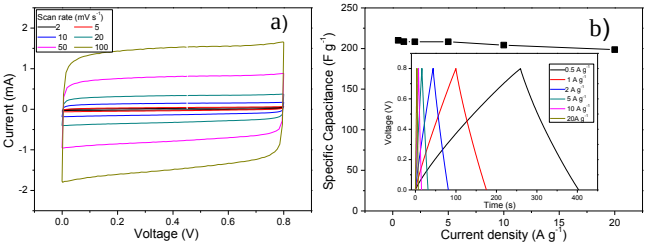

Fig. 6a) CV curves of VACNTs@MnO_2/CC at different scan rates ranging from 2 to 100 mV s^{-1}; (b) Specific capacitance of VACNTs@MnO_2/CC as a function of current densities, and the inset presents GCD curves from 0.5 A g^{-1} to 20 A g^{-1}.

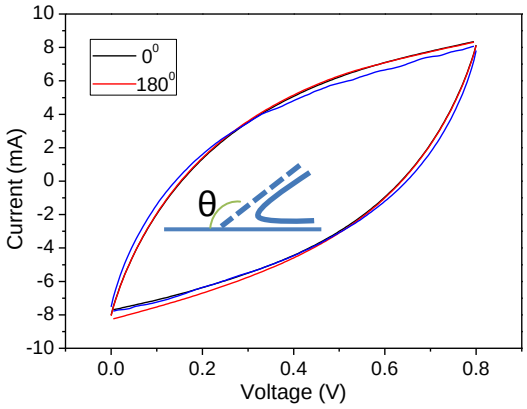

Fig.7 CV curves of flexible supercapacitor based on VACNTs@MnO_2/CC at 0° and 180° deformation at 50 mV s^{-1}.

The high performance of the VACNTs@MnO_2/CC electrode highly depended on its special structure. Because of the small thickness and the porosity of MnO_2 nanosheets as well as the arrayed structured of VACNTs@MnO_2/CC, the electrolyte can easily approach the surface of MnO_2, thus the redox reactions of MnO_2 can readily occur. On the other hand, the VACNTs connecting MnO_2 can transport the electrons for the redox reactions of MnO_2, which further increased the rate capacitance of the VACNTs@MnO_2/CC electrode. As a result of the good reversibility of VACNTs@MnO2/CC's redox reactions, the excellent cycling performance can be observed. The growth of CNTs on CC also played an important role in determining the good flexibility of the VACNTs@MnO_2/CC electrode because of the firm connection between CNTs and CC.

Experimental

Materials and methods

All the chemicals used were of analytical grade without further purifications. VACNTs arrays were grown on CCs (~2×2 cm^2) using a DC–biased plasma enhanced chemical vapour deposition (PECVD) system (AIXTRON) according to previous procedures.[40-43] Firstly, 10 nm thick Ni film was sputtered on the CCs by e-beam vapor system (Edwards BOC 500). After that, NH_3 gas (99.99%,at 200 Sccm) was introduced in the PECVD reaction chamber heated to 750℃ while holding for 10 min at a pressure of ~12mbar， then the system was cooled to 720℃ and C_2H_2 gas (99.99%, 60 Sccm) was inlet at a pressure of ~12 mbar. The deposition time was 35min. After growth, the VACNTs-modified CCs were directly transferred into a 40-mL Teflon-sealed autoclave containing 35 ml 10 mM of $KMnO_4$ solution for growth of MnO_2 nanosheets. The autoclave was sealed and put into an oven and kept at 180℃ for 30 min. After the reaction completed, the autoclave was taken out and cooled down quickly to the room temperature by cooling water. Finally, the VACNTs@MnO_2/CC was taken out, rinsed with copious pure water and ethanol, and dried at 120℃ for 30 min. Mass of the VACNTs@MnO_2 thin film can be calculated by measuring the mass difference between the CC and VACNTs@MnO_2/CC.

Characterizations

The scanning electron microscopy (SEM) images were obtained by using a FEI, NOVA NanoSEM430 microscope. Transmission electron microscopy (TEM) observations were performed on Tecnai G2 F20 U-TWIN instrument operated at 200 kV. The X-ray diffraction (XRD) data were collected using a Rigaku, Smartlab X-ray diffractometer with Cu Kα radiation (λ = 0.154178 nm). X-ray photoelectron spectroscopy (XPS) spectra were measured using an ESCALab 250 electron spectrometer from Thermo Scientific Corporation.

Electrochemical measurements

The electrochemical performances of the CNTs-modified CC and VACNTs@MnO_2/CC were carried out on VMP3 Potentiostat Galvanostat (EG&G, Princeton Applied Research) using a three-electrode cell system and two-electrode cell system, respectively. For three-electrode cell system, a Pt foil and a saturated calomel electrode (SCE) were served as the counter electrode and reference electrode, respectively, the CNTs-modified CCs or VACNTs@MnO_2/CC as the working electrode, and aqueous solution of 1.0 M Na_2SO_4 as electrolyte at room temperature. Electrochemical measurements of two-electrode system were carried out in a Swagelok-type cell with two symmetrical VACNTs@MnO_2-modified CCs electrodes with a glass fiber as separator (Whatman Cat No.1823 047), gold foils as current collector, and 1.0 M Na_2SO_4 as electrolyte. Cyclic voltammetry (CV) measurements were performed in the potential range of 0 to 0.8 V (vs.SCE) at various scan rates from 2 to 100 mV s^{-1}. Galvanostatic charge-discharge (GCD) measurements were carried out at different current densities varying from 0.5 A g^{-1} to 20 A g^{-1}. Electrochemical impedance spectra (EIS) were measured with a sinusoidal wave with a 5 mV amplitude at an open circuit potential in 1.0 M Na_2SO_4 electrolyte with frequencies spanned from 0.01 Hz to 100 kHz. The specific capacitances were calculated from CV and galvanostatic charge-discharge curves according to the following two equations respectively:

$$C = \frac{\int_a^b I(V)dV}{2 \times \Delta V \times \upsilon \times m}$$

$$C = \frac{I \times \Delta t}{m \times \Delta V}$$

where $\int_a^b I(V)dV$ is the integrated area of CV curve in one cycle, υ is the scan rate, I is the constant discharge current, Δt is the discharging time, ΔV is the potential window, and m is the mass of VACNTs@MnO_2 thin film.

Conclusions

In the study, we have constructed a new structure of vertical alligned CNTs@MnO_2 arrays on carbon cloth for flexible supercapacitor electrodes. The SEM and TEM characterizations of this composite reveal the presence of the core-shell structure. The electrochemical measurements of the VACNTs@MnO_2 on carbon cloth shows that this electrode exhibit a remarkable specific capacitance of ~235 F g^{-1} at the scan rate of 2 mV s^{-1}, an excellent rate performance with a specific capacitance of 188 F g^{-1} even at 100 mV s^{-1} and a stable cycling ability (nearly 100% retention after 5000 charge/discharge cycles at 5 Ag^{-1}). The flexibility of VACNTs@MnO_2-based symmetric supercapacitor is very good even if the superacapacitor is bent for 180°. The excellent performances in electrochemical properties and flexibility mainly originated from a strong mechanical coupling between CNTs and CC as well as the sufficient contact between electrolyte and the surface of MnO_2 nanosheets in such an arrayed structure. This new VACNTs@MnO_2 material on carbon cloth provides a new opportunity for constructing flexible electrical energy storage devices in near future.

Acknowledgements

The authors acknowledge the grants from National Basic Research Program of China (No.2012CB933402) and the National Key Scientific Instrument and Equipment Development Projects of China (No.2014YQ090709). We also appreciate Dr. Y-J. Guo and Dr. P. Xu for their valuable assistances.

References

1 P. Simon, Y. Gogotsi, *Nat. Mater.* 2008, **7**, 845.
2 L. Hu, W. Chen, X. Xie, N. Liu, Y. Yang, H. Wu, Y. Yao, M. Pasta, H. N. Alshareef, Y. Cui, *ACS Nano*, 2011, **9**, 5636.

3 X.L. Wang, G.Q. Shi, *Energy Environ. Sci.*, 2015, **8**, 790
4 S. Shi, C.J. Xu , C. Yang, J. Li, H.D. Du, B.H. Li, F.Y. Kang, *Particuology*, 2013,**11**,371
5 H, Gao, K. Lian, *RSC Adv.*, 2014,**4**, 33091
6 D.S. Yu, Q.H. Qian, L. Wei, W.C. Jiang, K.L. Goh, J. Wei, J. Zhang, Y. Chen, *Chem. Soc. Rev.*, 2015,**44**, 647
7 S.-C. Hong, S. Kim, W.-J. Jang, T.-H. Han, J.-P. Hong, J.-S. Oh, T. Hwang, Y. Lee, J.-H. Lee, J.-D. Nam, *RSC Adv.*, 2014, **4**, 48276.
8 Y. Zhang, Z. Guo, *Chem. Commun.*, 2014, **50**, 3443.
9 T.T. Liu, G.J. Shao, M.T. Ji, Z.P. Ma, *Asian J. Chem.* 2013,**25**,7065
10 W. Wei, X. Cui, W. Chen, D. G. Ivey, Chem. Soc. Rev., 2011,40, 1697.
11 S. Chen, J. W. Zhu, X. Wang, *Acs Nano* 2010, **4**, 6212.
12 L. L. Peng, X. Peng, B. R. Liu, C. Z. Wu, Y. Xie, G. H. Yu, *Nano Lett.* 2013, **13**, 2151.
13 P. H. Yang,; Y. Ding, Z. Y. Lin, Z. W.Chen, Y. Z. Li, P. F. Qiang, M. Ebrahimi, W. J. Mai, C. P. Wong, Z. L.Wang, *Nano Lett.* 2014, **14**, 731.
14 Z. J. Fan, J. Yan, T. Wei, L. J. Zhi, G. Q.Ning, T. Y. Li, F. Wei, *Adv. Func. Mater.* 2011, **21**, 2366.
15 G. H. Yu, L. B. Hu, N. A. Liu, H. L. Wang, M. Vosgueritchian, Y. Yang, Y. Cui, Z. A. Bao, *Nano Lett.* 2011, **11**, 4438
16 C. Wu, S. Deng, H. Wang, Y. Sun, J. Liu, H. Yan, *ACS Appl. Mater. Interfaces*, 2014**, 6**, 1106.
17 Jaidev, R. I. Jafri, A. K. Mishra, S. Ramaprabhu, *J. Mater. Chem.*, 2011, **21**, 17601.
18 Z. Zhang, F. Xiao, L. Qian, J. Xiao, S. Wang, Y. Liu, *Adv. Energy Mater.* 2014, **4**, 1400064.
19 G. Zhu, Z. He, J. Chen, J. Zhao, X. Feng, Y. Ma, Q. Fan, L. Wang, W. Huang, *Nanoscale*, 2014,**6**, 1079.
20 Y. Hou, Y. Cheng, T. Hobson, J. Liu, *Nano Lett.*, 2010, **10**, 2727.
21 L. Li, Z. A. Hu, N. An, Y. Y. Yang, Z. M. Li, H. Y. Wu, *J. Phys. Chem. C* 2014, **118**, 22865.
22 P. Lv, Y. Y. Feng, Y. Li, W. Feng, *J. Power Sources*,2012, **220**, 160.
23 L. Bao, J. Zang, X. Li, *Nano Lett.* 2011, **11**, 1215.
24 A. A. Radhiyah, M. Izan Izwan, V. Baiju, C. Kwok Feng, I. Jamil,R. Jose, *RSC Adv.*, 2015,**5**, 9667.
25 F. Li, Y. Xing, M. Huang, K.L. Li, T. T. Yu, Y. X. Zhang, D. Losic, J. *Mater. Chem. A*, 2015,**3**, 7855.
26 Y. Jiang,X. Ling, Z. Jiao, L. Li , Q. Ma, M. Wu, Y. Chu, B. Zhao,*Electrochimica Acta* ,2015,**153**, 246.
27 X. Feng, Z. Yan, N. Chen, Y. Zhang, Y. Ma, X. Liu, Q. Fan, L. Wang, W. Huang, J. Mater. Chem. A, 2013,**1**, 12818.
28 D. Guo, X. Yu, W. Shi, Y. Luo, Q. Li, T. Wang, *J. Mater. Chem. A*, 2014,**2**, 8833.
29 X. Wang, H. Liu, X. Chen, D. G. Evans, W. Yang, *Electrochimica Acta*,2012, **78**, 115
30 D. Guo, Y. Luo, X. Yu, Q. Li, T. Wang, *Nano Energy*, 2014,**8**,174
31 P. Srimuk, S. Luanwuthi, A. Krittayavathananona, M. Sawangphruk, *Electrochimica Acta*, 2015, **157**,69.
32 D. L. Ji, J. H. Li, L. M. Chen, D. Zhang, T. Liu, N. Zhang, R. Z. Ma, G. Z. Qiu, X. H. Liu, *RSC Adv.*, 2015,**5**, 41627.
33 H. Xia, M.O. Lai, L. Lu, *J. Mater. Chem.* 2010, **20**, 6896.
34 Z. B. Lei, F. H.Shi, L. Lu, *Acs Appl. Mater. Inter.* 2012, **4**, 1058.
35 G. H. Yu, L. B. Hu, M. Vosgueritchian, H. L. Wang, X. Xie, J. R. McDonough, X. Cui, Y. Cui, Z. N.Bao, *Nano Lett.* 2011, **11**, 2905.
36 P. X. Li, Y. B. Yang, E. Z. Shi, Q. C. Shen, Y. Y. Shang, S. T. Wu, J. Q. Wei, K. L. Wang, H. W. Zhu, Q. Yuan, A. Y. Cao, D. H. Wu, *Acs Appl. Mater. Inter.* 2014, **6**, 5228.
37 H. J. Wang, C. Peng, J. D. Zheng, F. Peng, H. Yu, *Mater. Res. Bull.* 2013, **48**, 3389.
38 R. Kötz, M. Carlen, *Electrochimica Acta*, 2000, **45**, 2483.
39 S. Yoon, C. W. Lee, S. M. Oh, *J. Power Sources*, 2010,**195**, 4391.
40 M.S. Haque, K.B.K. Teo, N.L. Rupensinghe, S. Z. Ali, I. Haneef, S. Maeng, J. Park, F. Udrea, A.I. Milne, *Nanotechnology,* 2008, **19**, 025607
41 X. Jin, W. Zhou, S. Zhang, G. Z. Chen*, Small,* 2007, **3**, 1513.
42 J. W. Liu, J. Essner, J. Li, *Chem. Mater.* 2010, **22**, 5022.
43 B.Hsia, J. Marschewski, S. Wang, J. B. In, C. Carraro, D. Poulikakos, C. P. Grigoropoulos, R. Maboudian, *Nanotechnology,* 2014, **25**, 055401

Graphical Abstract

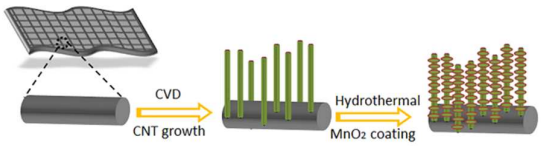

The VACNTs@MnO_2 arrays grown on carbon cloth can act as the high performance flexible electrode for supercapacitors.